Available online at www.sciencedirect.com

ScienceDirect

Procedia Structural Integrity 39 (2022) 528–545

Structural Integrity Procedia

www.elsevier.com/locate/procedia

7th International Conference on Crack Paths

Crack tip position evaluation and Paris' law assessment of a propagating crack by means of temperature-based approaches

Rosa De Finis [a*], Davide Palumbo [a], Francesca Di Carolo [a], Mauro Ricotta[b], Giovanni Meneghetti[b], Umberto Galietti [a]

[a]*Department of Mechanics, Mathematics and Management, Politecnico di Bari, Bari 70125, Italy*
[b]*Department of Industrial Engineering, University of Padova, Padova 35122, Italy*

Abstract

This paper investigates the possibility to evaluate the crack tip position, crack growth rate and stress intensity factor (SIF), in order to derive the Paris law by starting from the temperature distribution measured by means of an infrared camera, with high geometrical resolution. In more detail, constant amplitude, fully reversed, stress controlled, crack propagation fatigue tests were carried out on two single edge notch tension specimens machined from 4-mm-thick, hot-rolled AISI 304L stainless steel sheets.
The temperature maps were then processed by using a signal reconstruction algorithm based on the least square method in order to extract the maps of the amplitude and phase signal components of the first and second harmonics. In particular, the amplitude maps of the thermoelastic signal allowed the estimation of the stress intensity factor (SIF) using well-established methods, while the thermoelastic phase and second harmonic phase maps were used for estimating the crack-tip position. As for the determination of the crack tip using the phase maps, an experimental approach based on the evaluation of the inversion point of a phase profile (parallel to the crack propagation direction) was adopted. Such a point would represent the beginning of the reverse plasticity zone in the first and second harmonics phase maps.
The crack tip position based on temperature maps was systematically compared to that measured by means of a digital microscope. Similarly, experimental SIF values derived from the thermoelastic signals were compared with the relevant numerical values from linear elastic FE analyses. The resulting Paris laws were critically compared. The good agreement between the preliminary data suggest further investigations regarding the applicability of these methods in all load conditions.

Keywords: Temperature approaches; Energy approaches; Thermoelastic Stress Analysis; Stress Intensity Factor range; Mode I.

10.1016/j.prostr.2022.03.126

* Corresponding author. Tel.: +39 333 43 50 585.
E-mail address: rosa.definis@poliba.it

1. Introduction

The process of fatigue failure can be described by the initiation and growth of cracks under cyclic loading, so that the evaluation and prediction of fatigue crack growth (FCG) represent an essential part of failure prevention and control (Kumar Paul(2012)). In this way, the stress state in the vicinity of the crack tip can be determined via the assessment of the Stress Intensity Factor (SIF) that characterizes the magnitude of the stresses in the proximity of an ideally sharp crack tip in a linear-elastic and isotropic material. It plays an important role in the investigation of the behaviour of cracked brittle components and structures. As an example, crack growth rate dependence on SIF provides the basis for fatigue lifetime estimation of cracked components (Dowling (2020)).

Different approaches were set up to evaluate SIF (Yates (2010), Vasco-Olmo (2016),Stanley (1997), Tomlinson (1997), Tomlinson (1999), Dulieu-Burton,(2003), Diaz (2004), Diaz, (2004), Tomlinson (2011), Diaz (2013), Meneghetti and Lazzarin (2007), Lazzarin et al (2010), Palumbo et al (2015), Pitarresi et al (2019)) . Meneghetti and Lazzarin (2007), proposed an expression useful to estimate the notch stress intensity factor (NSIF) from finite element analyses carried out by using a mesh pattern with a constant element size. By using this approach, the analysis required only the evaluation of elastic peak stress at the V-notch tips using rather coarse meshes if compared to those from usual analyses focused on evaluating the whole local stress field.

Lazzarin et al. (2010), adopted and energetic approach based on strain energy density (SED) assessment and discussed the link between local SED and NSIFs for welded joints and sharp V-notched plates to determine theoretical stress concentration factor.

From an experimental point of view, SIF ranges and crack tips can be assessed by adopting TSA (Thermoelastic Stress Analysis) (Diaz (2004), Diaz, (2004), Tomlinson (2011), Diaz (2013)). TSA as a thermography-based technique Stanley (1997), requires an ease surface preparation involving just the application of a matt black to ensure high and uniform surface emissivity. Such an approach is useful during in-service applications on real components under cycling loading conditions and provides useful parameters to investigate the material behaviour near the plastic region.

By considering that the heat generation due to plastic work and the presence of high stress gradients phenomena occur near the crack tip region one can use the thermoelastic phase signal data to determine the position of the crack tip when it returns to zero from negative values representing a plastic zone boundary (Tomlinson (2011)). In recent work, Palumbo et al (2015) and Pitarresi et al (2019), proposed the use the second-harmonic of thermal signal in terms of phase to evaluate the crack tip.

The capability of TSA is also in the estimating the SIF range. The technique, in effect, provides also the full field map of the first stress invariant that can be used as an useful information to evaluate fracture mechanics parameters. Stanley (1997), proposed a procedure based Westergaard' equations for elastic plane stress and elastic plane strain conditions where a direct interpolation method provided the SIF under mode I loading. SIF represented the coefficient of proportionality between inverse squared of maximum thermoelastic signal and the distance from the crack line. This procedure does not require the exact identification of the crack tip, but on the other side it neglects another parameter important to describe the stress state in proximity of the crack tip, the T-stress (Gupta, (2015)).

Other approaches (Vasco-Olmo et al (2016), Tomlinson et al (2011), Diaz, (2004), Lesniak (1995)) adopted Over-Deterministic Methods (ODMs) based on Least Square Fitting (LSF) of analytical stress functions to assess the elastic stress field near the crack. Lesniak et al. (1995) as an example, adopted Williams' stress solution for measuring the mixed-mode stress intensity factor of isotropic materials and the results exhibited errors up to 20% in the mixed-mode stress intensity factor measurements. To reduce these errors, Tomlinson et al.(1997) presented an alternative methodology to determine the SIF for cracks under mixed-mode displacements. In this case, the stress field was described using Fourier series according to Muskhelishvili's complex potentials approach. Pitarresi et al (2019), adopted Williams' approach to investigate the influence of the series terms number, the selection of the fitting area and the crack tip location on the SIF evaluation.

Accounting for Stanley-Chan' direct interpolation method and Over-Deterministic approach, in this research the crack-tip stress fields of two Single Edge Notched Tension (SENT) samples made of AISI 304 steel under fully reversed loading, have been studied in order to evaluate the crack tip positions, crack growth rates and stress intensity factors (SIFs). The Paris' laws via only thermoelastic data were derived. The aims of the research were firstly to compare the crack tip positions and stress intensity factor ranges found via different TSA-based methods and secondly to discuss the capability of different methods in estimating the Paris' law.

Nomenclature

a, b	Thermoelastic parameters
A_{I3}	the third term of Williams' solution
C_ε	Specific Heat at constant strain
E	Young' modulus
f	loading frequency
K_I	Stress Intensity Factor mode I
K_{Imax}	Maximum value of the Stress Intensity Factor
K_{Ia}	Amplitude value of the Stress Intensity Factor
R	Stress ratio
r, θ	Polar coordinates
s	First stress invariant
$\dot{s}$	First stress invariant rate
T_s	T-stress
T_0	Reference temperature
$\dot{T}$	Temperature variation rate
α	Coefficient of linear thermal expansion
ΔK_I	Stress Intensity Factor range
ΔT_1	Thermoelastic amplitude signal
ρ	Density
σ_i	Principal stress
$\dot{\sigma}_1$	Principal stress rate
σ_{mi}	Mean uniaxial stress along i direction
σ_{ai}	Amplitude uniaxial stress along i direction
υ	Poisson's ratio
φ1	first-harmonic phase (thermoelastic phase shift)
φ2	second-harmonic phase
CGR	Crack growth rate (*da/dN*)
ODM	Over-deterministic method
SENT	Single Edge Notch Tension
SIF	Stress Intensity Factor
TSA	Thermoelastic Stress Analysis

2. Theory

The thermoelastic effect (William Thomson, (1878)) relates the temperature change with the change in the sum of principal stresses for an isotropic material in linear elastic and adiabatic conditions. In particular, temperatures and stresses are related by the thermoelastic constant that is generally assumed to be constant independently on the applied stress.

For an isotropic material without any internal heat source, the temperature variations are related to the first stress

invariant and principal stresses:

$$\rho C_\varepsilon \frac{\dot{T}}{T} = -\left[\alpha + \left(\frac{\upsilon}{E^2}\frac{\partial E}{\partial T} - \frac{1}{E}\frac{\partial \upsilon}{\partial T}\right)s\right]\dot{s} + \left[\frac{(1+\upsilon)}{E^2}\frac{\partial E}{\partial T} - \frac{1}{E}\frac{\partial \upsilon}{\partial T}\right]\sigma_i\dot{\sigma}_i \quad (1)$$

Where ρ is the material density, C_ε is the specific heat under constant strain, T is the temperature , σ_i are principal stresses, υ is the Poisson modulus, s is the first stress invariant, E is the Young modulus and α is the linear thermal expansion coefficient.

The material constants, a and b, are defined in (Patterson et al. (2007) , Palumbo et al. (2015) and Di Carolo et al. (2019)) and the principal stresses can be written as:

$$\sigma_1 = \sigma_{a1}(R_f + sin\omega t)\text{,}\ \ \sigma_2 = \sigma_{a2}(R_f + sin\omega t) \quad (2)$$

where ω is the angular frequency and σ_{ai} are the amplitude of uniaxial stress along the generic i direction.

Under a generic sinusoidal loading in which the load changes between its maximum and minimum values, P_{min} and P_{max}, the loading ratio R can be defined as:

$$R = \frac{P_{min}}{P_{max}} = \frac{\sigma_{i,min}}{\sigma_{i,max}}, \qquad \sigma_{mi} = \sigma_{ai}\frac{1+R}{1-R} = \sigma_{ai}R_f \qquad \text{with } i=1,2 \quad (3)$$

By deriving the Eq. (2) and substituting them in Eq. (1), it leads:

$$\frac{\dot{T}}{T} = \left[-a(\sigma_{a1} + \sigma_{a2}) + bR_f(-2\nu\sigma_{a1}\sigma_{a2} + {\sigma_{a1}}^2 + {\sigma_{a2}}^2)\right]\omega\, cos\, \omega t + [b(1+2\nu)({\sigma_{a1}}^2 + {\sigma_{a2}}^2) + +2\nu b\sigma_{a1}\sigma_{a2}]\omega\, sin\, \omega t\, cos\, \omega t \quad (4)$$

By integrating Eq. (4) , considering $\Delta T \ll T_0$ and neglecting the static components, the general expression of the thermoelastic signal in proximity of the crack can be written as:

$$\frac{\Delta T\,(t)}{T_0} = g_1 \sin\omega t + g_2 \cos 2\omega t \quad (5)$$

where:

$$g_1 = \left[-a(\sigma_{a1} + \sigma_{a2}) + bR_f(-2\nu\sigma_{a1}\sigma_{a2} + {\sigma_{a1}}^2 + {\sigma_{a2}}^2)\right], \quad (6a)$$

$$g_2 = -\frac{1}{2}[b(1+2\nu)({\sigma_{a1}}^2 + {\sigma_{a2}}^2) + 2\nu b\sigma_{a1}\sigma_{a2}] \quad (6b)$$

By focusing on the component $g1$ provided by Eq. (6b), considering the only mode I of loading, and combining Eq. (5) with Westergaard solution (Stanley, (1997)) and putting $b=0$, after few mathematical steps gives:

$$\Delta T_{west}(\mathrm{r}) = g_1 T_0 = -T_0\left(\frac{2aK_{Ia}}{\sqrt{2\pi r}}\cos\frac{\theta}{2} + \sigma_{0x}\right) \quad (7)$$

Eq. (7) represents the classical solution used for relating the thermoelastic signal and K_{Ia}, where the SIF range is:

$$K_{Ia} = K_{Imax}\left(\frac{1-R}{2}\right) = \frac{\Delta K_I}{2} \tag{8}$$

By combining the general expression of the thermoelastic signal, Eq. (5) with Williams' series expansion (Lesniak et al (1995)) truncated to the third term and putting $b=0$, it leads to obtain the following:

$$\Delta T_{will,}(r) = g_1 T_0 = a\left[-cos\left(\frac{\theta}{2}\right)\left(2A_{I3}\sqrt{r} + \frac{KI_a\sqrt{2}}{\sqrt{\pi}}\right) - T_s\right] \tag{9}$$

Eq. (9) is the classical solution used for relating the thermoelastic signal and K_{Ia} when describing the local stress state in the proximity of the crack tip with Williams' formulation.
In the next section, the experimental campaign and methods adopted for estimating crack tip, crack growth rate and SIF ranges will be shown.

3. Experimental campaign and thermal data processing

Two SENT samples have been tested under constant amplitude, fully reversed (R=-1), load controlled crack propagation fatigue tests. The samples were prepared from 4-mm-thick, hot-rolled AISI 304L stainless steel sheets, the geometry is represented in Fig. 1. The machined V-notch samples presented a notch radius of 0.1 mm and a notch opening angle of 45°. The distance between grips was 90.00 mm.
After the natural crack starting from the V-notch under the fatigue loading, the fatigue crack propagation was monitored by infrared camera and optical microscope each one observing the sample surface on opposite sides. The setup is the same of the one presented in Meneghetti et al (2019).

The material surface temperature was measured by using a FLIRSC7600 infrared camera, equipped with an analog input interface, which was used to synchronize the force signal from the load cell with the temperature signal measured by the infrared camera. The infrared camera operated at a frame rate equal to 200 Hz. A 30-mm spacer ring was adopted to improve the spatial resolution and achieve 23 μm/pixel (Pitarresi et al (2019), Meneghetti et al (2019)).
The sample face exposed to the IR camera was painted with a matt black paint in order to improve and make uniform the infrared emissivity. Each acquired thermal sequence had a duration of 5 sec.

Thermal data were processed by using the MotionByInterpolation tool to reduce the effect of relative motion between the fixed camera lens and the moving specimen due the sinusoidal applied load.
After this preliminary analysis the infrared images, a signal reconstruction algorithm was adopted according to the procedure presented in the work of De Finis et al (2017) and Ancona et al. (2016), in order to extract the maps of the thermal signal components: ΔT_1 thermoelastic signal map useful for the estimation of the stress intensity factor range, φ_1 and φ_2 respectively the first-harmonic (thermoelastic) and second-harmonic phase shifts of thermal signal. The raw data maps were addressed to a 2D gaussian data smoothing to reduce the noise (De Finis et al (2017)) . The maps of parameters ($\Delta T_{1,}$ φ_1 , φ_2) considered for the analyses are shown in Fig. 2(a)-(b)-(c).
The adopted digital microscope was the Dino-lite AM4115ZT operating with a magnification ranging from 20x to 220x. The micrographs were used to obtain a reference the crack-tip position.

The tables containing all the information on the tests (loading frequency, number of cycles acquired and imposed gross-section stress amplitude $\sigma_{a,gross}$) is shown in Table 1.

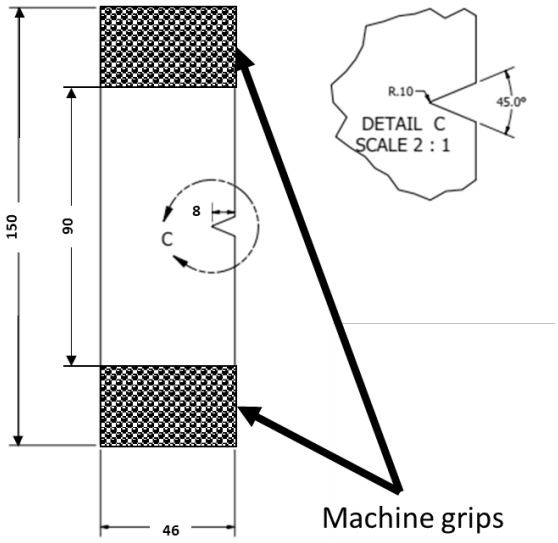

Fig. 1. (a) sketch of the geometry of V -notch samples (dimensions in mm).

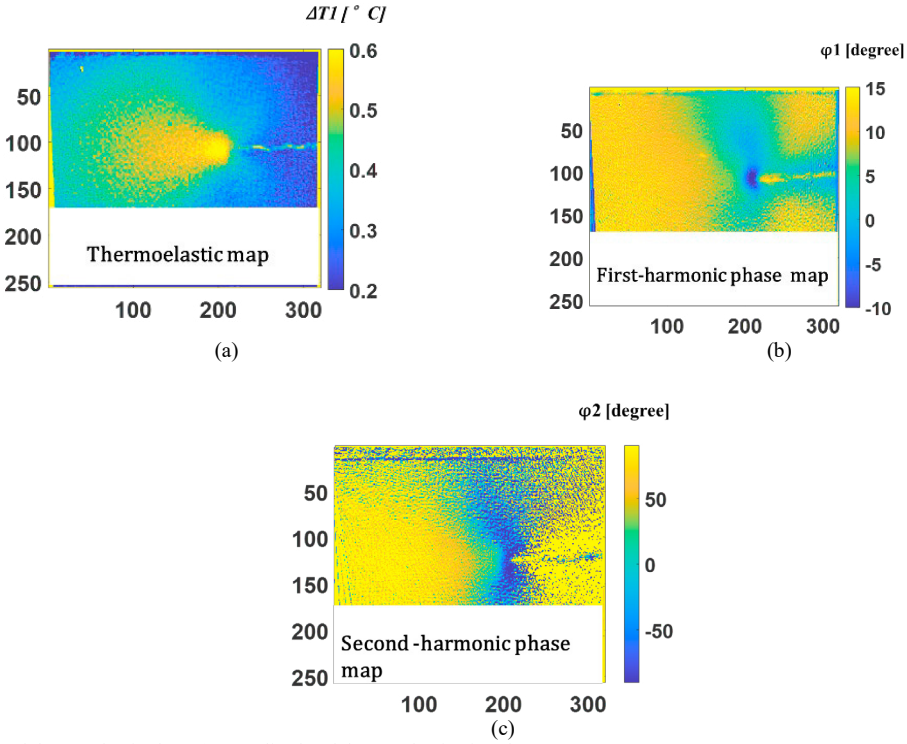

Fig. 2. Maps of thermoelastic data: (a) amplitude of thermoelastic signal, ΔT_1, (b) first-harmonic (thermoelastic) phase shift φ_1 and (c) second-harmonic phase shift φ_2.

Table 1. Input parameters for testing (a) sample 1 and (b) sample 2.

(a)

sample	Analysed sequences	f [Hz]	Acquired cycles	R	σa,gross [MPa]
1	1	40	76339	-1	52.63
	2	40	104030		
	3	40	158770		
	4	40	179485		
	5	40	227593		
	6	40	238960		
	7	40	243910		
	8	40	247627		
	9	30	263170		

(b)

sample	Analysed sequences	f [Hz]	Acquired cycles	R	σa,gross [MPa]
2	1	10	1281	-1	100
	2	25	4549		
	3	27	10776		
	4	30	15678		
	5	30	21393		
	6	30	25165		
	7	30	33159		
	8	10	44135		
	9	10	46735		

4. Data analysis and adopted methods

In present section the adopted methods for estimating crack tip, crack growth rate and stress intensity factor range (ΔK_I) are presented. In order to provide a clear overview of the analyses carried out and their outputs, a workflow of the adopted methods is presented in Fig. 3.

The optical microscope installed in front of the samples provided the reference values of the crack tip estimations. Even if it was scanning the opposite face of the sample, it has been assumed that it provided a reasonable estimation of the crack tip positions with good accuracy. By coupling the information of crack tip positions and loading cycles, and applying the secant method (ASTM E647, 2004), the crack growth rate (CGR-*da/dN*) was estimated.

The reference value of ΔK_I was assessed by evaluating the elastic peak stress at the V-notch tip via numerical analyses using the procedure reported by Meneghetti and Lazzarin, (2007). The values of CGR and ΔK_I provided the Paris'-like law, called hereafter Paris'-like Law_FEM_OM to whom the others obtained Paris'-like laws were compared.

The following sections *4.1* and *4.2* report the methods using thermoelastic data to assess crack tip position and stress intensity factor range in order to obtain the Paris'-like Law_Stanley-Chan_φ_1/φ_2 and Paris'-like law obtained by combining the general expression of the thermoelastic signal and Westergaard' and Williams' formulations.

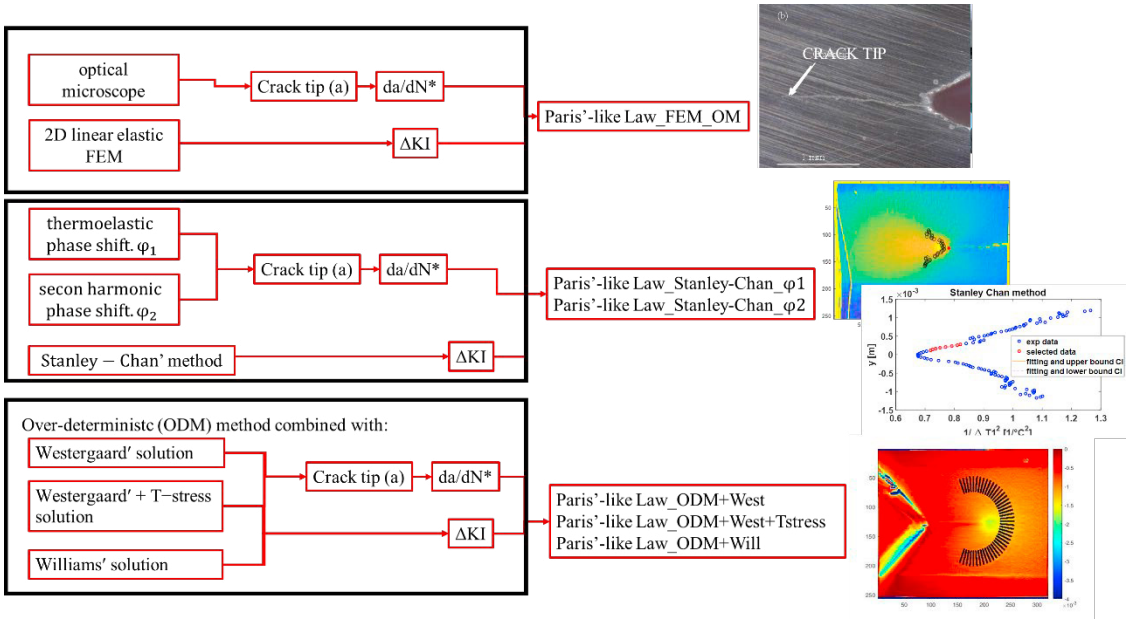

Fig. 3. Workflow of the adopted methods and carried out analyses.

4.1. Crack tip via thermoelastic phase maps and ΔK_I via Stanley-Chan' method

Thermoelastic phase shift represents the phase angle between thermoelastic and loading signal. It has been widely used for the fatigue crack growth evaluation (Stanley, (1997)).

In general phase angle remains locally constant in presence of linear elastic behavior but it can change due to plastic behaviour or high stress gradients leading to heat conduction and loss of adiabatic conditions. Near the crack tip region, two phenomena lead to loss of adiabatic condition: heat generation due to plastic work and high stress gradients. These phenomena determine a change in phase signal and then by analysing phase maps, the crack tip position can be evaluated (Tomlinson et al, (1999). Indeed, in proximity of the crack tip there is a positive increment of the phase value that indicates a loss of adiabatic condition due to plasticity and high stress gradients. Then the phase changes from positive to negative values, indicating a reverse plasticity, and then it returns to zero. Such a point has been empirically considered as a first estimate of the crack tip, (Tomlinson et al, (1999) and Palumbo et al (2015), Ancona et al (2016)).

In the work of Pitarresi et al, (2019), the use of the second-harmonic phase shift as parameter to determine the crack tip position was also proposed. More precisely, the phase inversion point seems to be related to the point which separates the plastic region and crack-closure zone. In present research, it was used to estimate the crack tip as well.

The procedure to estimate the crack point inversion in the φ_1 and φ_2 maps is quite simple. As represented in Fig.4a. it is preliminary necessary to estimate the coordinates of the maximum of thermoelastic signal (ΔT_1 map) in an area (A) surrounding the plastic zone, as described by Ancona, Ancona et al (2016). Such point provides the y-coordinate of the profile parallel to the crack growth direction where phase data are evaluated. However, before considering that profile, the phase data are scaled of the mean value (φ_{1mean} and $\varphi_{2\ mean}$) of a region where the material is under elastic conditions, so that sufficiently far away from the crack tip. This procedure allowed the reset of the average value of the phase signal to zero in the boundaries of plastic zone and far away from the crack tip where adiabatic conditions are achieved. By considering, then, the *y-max* profile in the φ_1 and φ_2 maps parallel to the crack growth direction, it is possible to observe the inversions points and then to find the crack tips, Fig. 4b. In Fig. 4b is also reported the ΔT_1 profile along the crack direction corresponding to the same y-coordinate where it is possible to observe that the maximum of thermoelastic amplitude signal occurs roughly in correspondence of the minimum of φ_1 profile.

As for the evaluation of the stress intensity factor range, Stanley-Chan (Stanley, (1997), Ancona et al, (2016)) presented a procedure based on Westergaard' solution for the elastic plane stress conditions where SIF range can be obtained adopting a direct interpolation method relating the first stress invariant and the distance from crack tip position. Specifically, it was found that, in pure Mode I, the maximum value of linear stress invariant (that is the sum of normal stresses), along a line parallel to the crack line and distant y from it, is linearly correlated to the distance y through the following relationship (Pitarresi et al, (2019)):

$$y = \left(\frac{3\sqrt{3}}{4\pi} T_0^2 K_{TSA}^2 \Delta K_I^2\right) \frac{1}{\Delta T_{1,max}^2} \tag{10}$$

By simply fitting the data of y versus $1/\Delta T_{1,max}^2$ lying in the SIF-dominated region (once K_{TSA}, the thermoelastic constant and T_0 the room temperature, are known), the slope of the linear model fitting represents ΔK_I. An excerpt of the method is presented in Fig. 4c where phase profile along the crack growth direction is overlapped to thermoelastic signal map. In the figure, the markers representing the points where the ΔT_1 is maximum are also presented: only those points lying in the SIF-dominated region have been taken into account to estimate the SIF-range according to Stanley-Chan' procedure.

The main advantage of the method is that only a series of signal profiles (horizontal or vertical) scanning around the crack-tip stress field and away from the plastic zone are required to obtain the SIF range measurement, hence the position of the crack tip is not required. The main drawback of the approach consists in neglecting of the T-stress in the Westergaard' formulation.

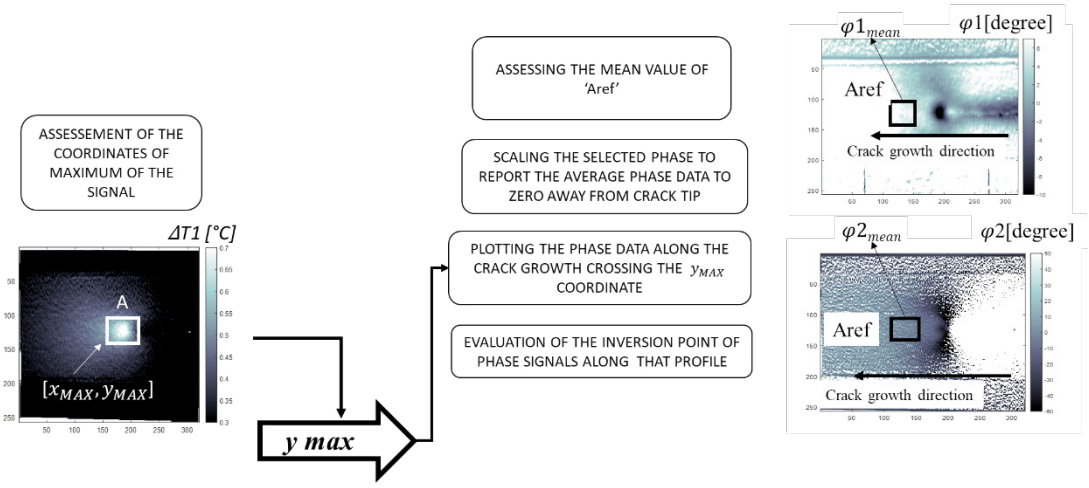

(a)

(b)

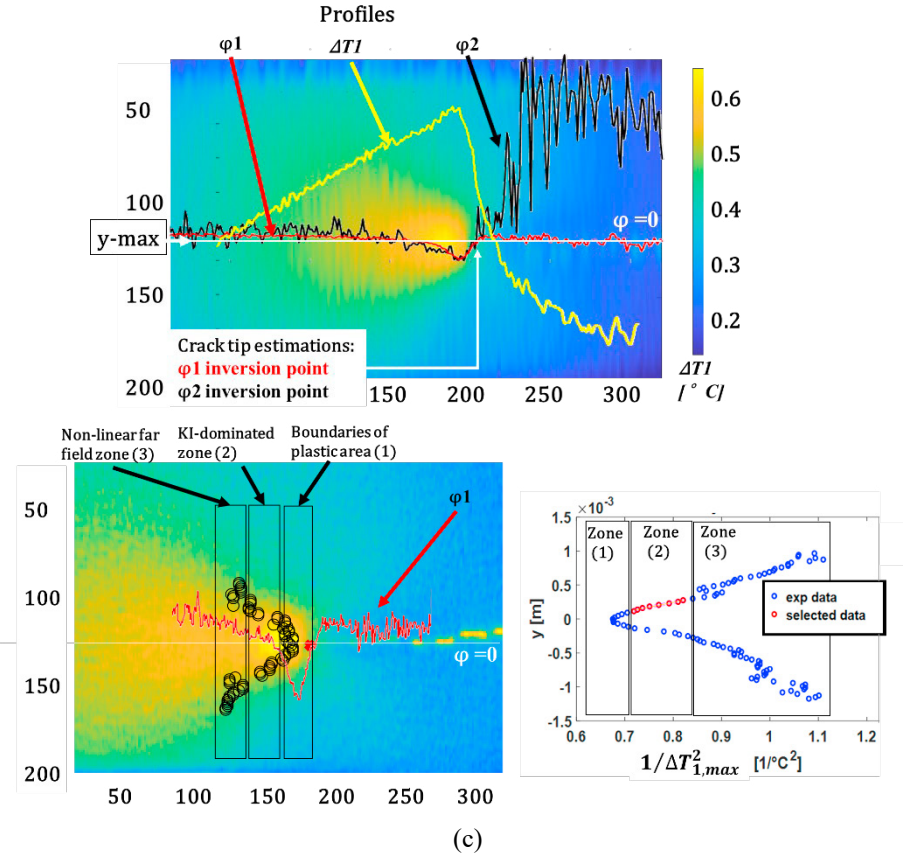

(c)

Fig. 4. Procedure to obtain the crack tip from φ_1 and φ_2 data.

4.2. Crack tip and ΔK_I via Over-deterministic approach

The data processing involved the application of the Last Square Over-deterministic method (Diaz et al, (2004)) to obtain the optimized crack tip coordinates and the value of the unknowns (ΔK_I, T_s, A_{I3}) of the system of equations(Eq. (7) and (9)).

The crack tip coordinates are optimized according to a procedure based on crack tip search in an area close to an initial guess. The crack tip point that minimizes the sum of deviations is selected. In order to implement such a procedure, the φ_1 data are employed to identify the crack tip initial value and plastic area boundaries. The crack tip initial was guessed at the point of φ_1 signal inversion profile (Diaz et al. (2004), Tomlinson et al (2011), Ancona et al, (2016)), (the same point adopted in section *4.1,* Fig. 4b). The plastic area was assumed to be characterized by negative phase values. This ensures that it could be in the worst case overestimated depending on loading frequency.

The minimum radius of the mesh starts when the phase values of the profile chosen returns to the zero value. After a semi annular mesh of points around the crack tip is created in the elastic zone.

As previously said, for each considered thermoelastic model (Eq. (7), Eq. (9)), an Over-deterministic System of equation can be written by substituting the ΔT_1 values of the mesh, together with other calibration parameters (*a*

Pitarresi et al (2019)), the loading conditions, and the polar coordinates in the models. The unknowns of this system are: ΔK_I in Westergaard' and ΔK_I, T_s and A_{I3} in Williams' formulations.

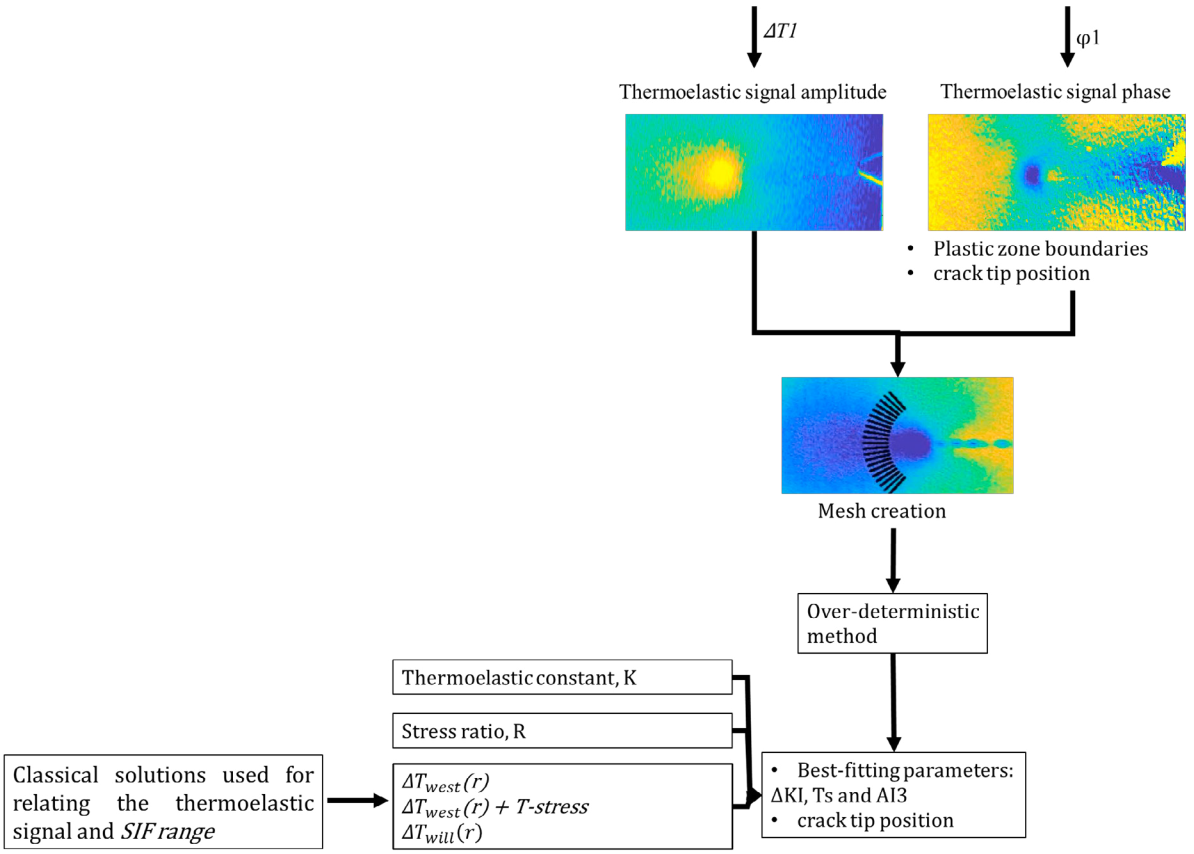

Fig. 5. Procedure to obtain the crack tip and ΔK_I using over-deterministic method: workflow.

5. Data analysis and adopted methods

In present section the results are shown in terms of crack tip positions, crack growth rate and ΔK_I and finally in terms of Paris' like laws.

5.1. Crack tip, crack growth rate and ΔKI evaluations

The crack tip assessed by using optical microscope has been compared to crack tips obtained by using the phase inversions points of φ_1 and φ_2 and those obtained by implementing the over-deterministic method.

The differences along the crack propagation direction are reported in Table 2 for the two samples.

By observing the results Table 2*a* is possible to observe that the crack tip positions found by TSA-based methods involve a maximum difference ranging between 0-0.55 mm, which leads to highlight the capability of methods in the assessment of the crack tip position. Moreover, the different methods provide crack lengths almost always shorter than those estimated by using optical microscope data.

As for sample 2, Table 2b reports quite different observations. In particular, some cracks are longer than the corresponding ones evaluated by using optical microscope, especially the crack lengths evaluated by considering the φ_1 and φ_2 inversion points. Moreover, the differences in the crack lengths compared to reference ones are broadly higher in some cases. However, the error made is 2.30 mm in the worst case.

Table 2. Differences in crack tips found by TSA-based methods and Optical microscope for (a) sample 1 and (b) sample 2.

Sample 1. Difference along crack propagation direction between crack tip x-coordinate of optical microscope and crack tip found by:

	φ_1-inversion point	φ_2-inversion point	TSA_ODM_West	TSA_ODM_West+Tstress	TSA_ODM_Will
			[mm]		
Sequence 1	0.41	0.18	0.09	0.09	0.09
Sequence 2	0.48	0.39	0.39	0.28	0.28
Sequence 3	0.41	0.30	0.41	0.09	0.09
Sequence 4	0.48	0.46	0.41	0.21	0.21
Sequence 5	0.55	0.53	0.55	0.55	0.48
Sequence 6	0.21	0.21	0.07	-0.07	-0.07
Sequence 7	0.53	-0.05	0.14	0.14	0.14

(b)

Sample 2. Difference along crack propagation direction between crack tip x-coordinate of optical microscope and crack tip found by:

	φ_1-inversion point	φ_2-inversion point	TSA_ODM_West	TSA_ODM_West+Tstress	TSA_ODM_Will
			[mm]		
Sequence 1	-0.53	-0.62	-0.37	-0.14	-0.14
Sequence 2	-0.18	-0.21	-0.21	0.09	0.09
Sequence 3	-0.28	-0.60	-0.35	0.25	0.25
Sequence 4	-0.67	-0.69	-0.07	-0.51	-0.53
Sequence 5	-0.16	-0.12	1.68	0.14	0.14
Sequence 6	-0.12	0.00	2.30	0.09	0.09
Sequence 7	-0.07	-0.35	2.05	0.12	0.12

Under graphic point of view, the following Fig. 6a-b report the thermoelastic signal maps together with the makers representing the positions of the crack tips found via different methods.

In Fig. 6a are reported the thermoelastic maps of sample 1 at different crack lengths. There is a good agreement between the crack tips found by using TSA-based methods and the reference (optical microscope) at different crack lengths and above all, all the methods allow to estimate the crack tip position with a good confidence. The same considerations can be drawn for sample 2, even if a major data scatter is observed in the crack tip positions especially when the crack length is higher.

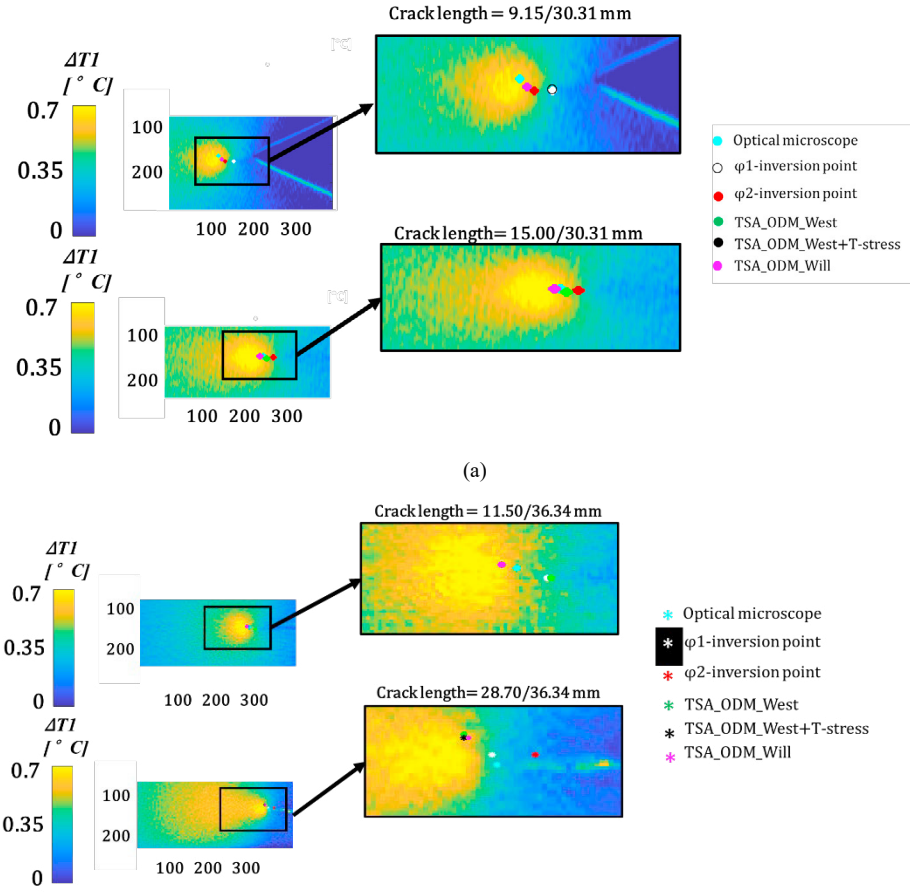

Fig. 6. Crack tip positions via TSA-based methods and optical microscope observations: (a) sample 1 and (b) sample 2.

By reporting the crack lengths versus the loading cycles for sample 1 (fig. 7a), as previously confirmed by the detected crack tip positions, a good agreement between the TSA-based methods is observed in comparison with reference crack lengths. In particular, a slight underestimation seems to be present for all the methods except for TSA_ODM+Will solution.

By comparing the CGRs compared to SIF range from FEM, Fig. 7b: a slight dispersion with respect to CGR from data obtained by optical microscope observations is highlighted. However, this effect can be improved by using the incremental polynomial method [ASTM E647, 2004] based on non-linear data fitting to obtain each CGR once the cycles are known.

In Fig. 8a, are reported the crack lengths compared to loading cycles, it is observed a a slight overestimation for TSA_ODM+Will data. As for CGRs compared to SIF range from FEM: a slight dispersion with respect to CGR from OM is observed in Fig. 8b.

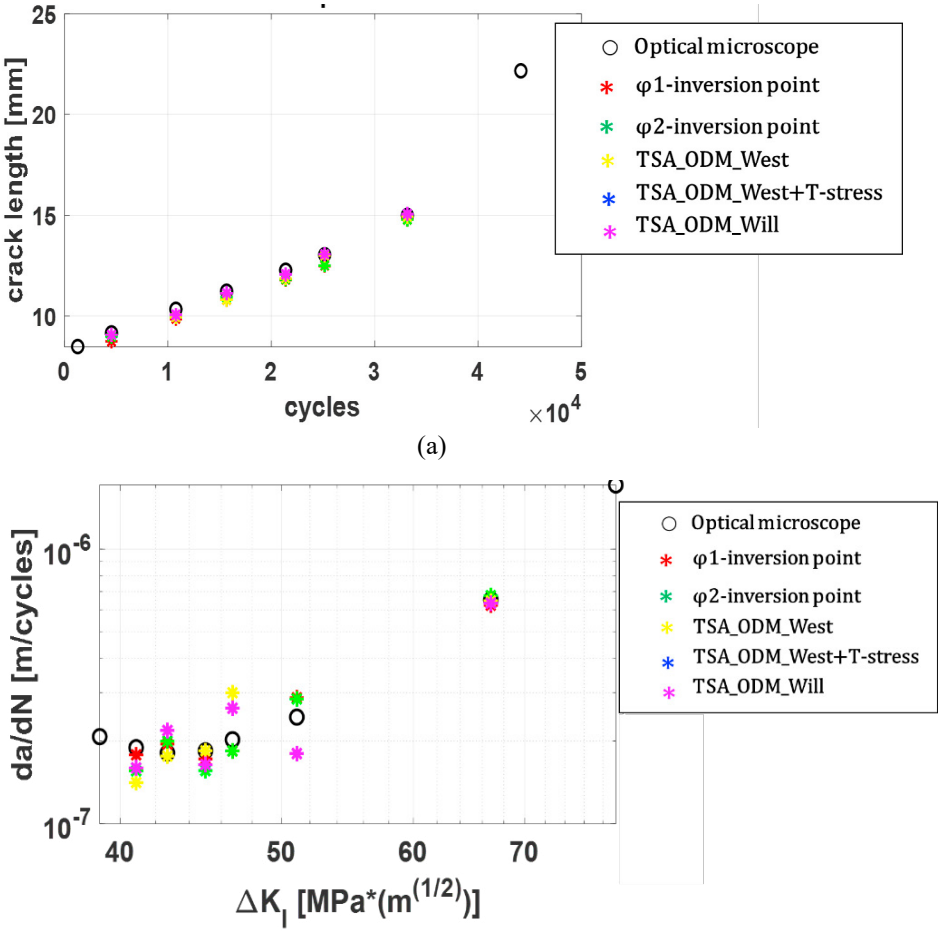

(a)

(b)

Fig. 7. Sample 1: (a) crack length versus loading cycles, (b) CGR versus ΔK_I obtained by FEM.

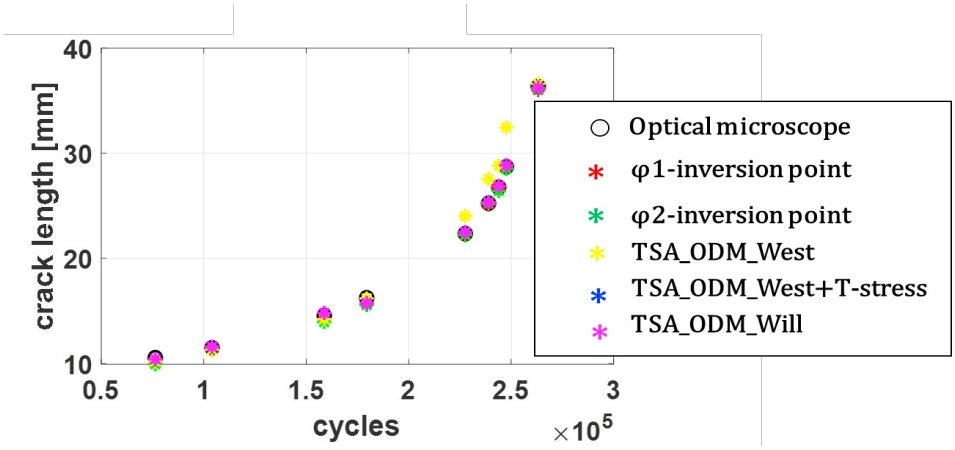

(a)

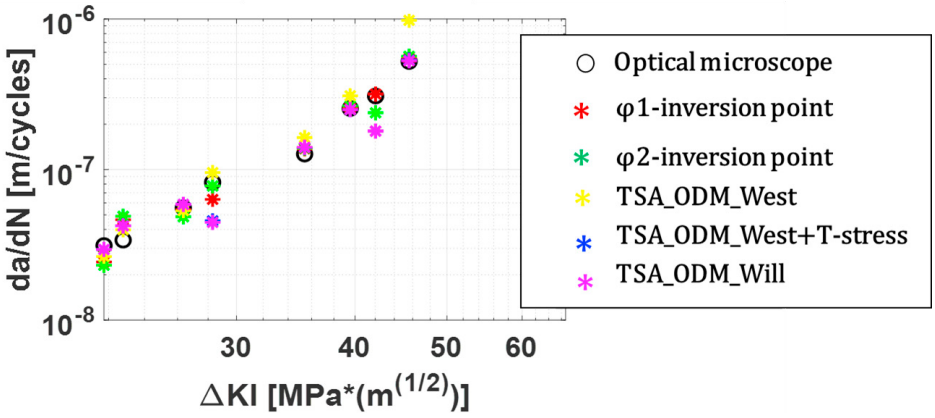

(b)

Fig. 8. Sample 2: (a) crack length versus loading cycles, (b) CGR versus ΔK_I obtained by FEM.

Finally, the comparison among the SIF range values is provided in Table III for the two samples. For sample 1 and (Table 3a-b), it is possible to observe that the SIF ranges from Stanley-Chan' method are quite in agreement with those obtained by numerical FEM analysis while over-deterministic methods provide lower values of SIF especially when combined with accurate formulations of Westergaard or Williams solutions taking into account the T-stress or more terms of the series. It is possible to observe that for sample 2 only SIF ranges obtained by considering Westergaard' formulation are in agreement with those provided by FEM, while TSA_ODM_West+T-stress and TSA_ODM_Will do not provide reliable values.

Such an underestimation could be ascribed to the determination of the boundaries of plastic area. In effect, a common drawback affecting over-deterministic least-square fitting-based methods is that it requires the crack tip location identification with high accuracy. However as presented before, the obtained crack tips are in good agreement with the one detected using optical microscope. Obviously, the stress intensity factor evaluations via ODMs are significantly influenced by the extension and position of the area used as input data with respect to direct interpolation methods. The selection of such an area is a trade-off between the fitting improvement and avoid being too close to the plastic area (Pitarresi et al, (2019)).

Another issue can be represented by the imposed stress ratio. Since in this case it determines a fully reversed load, the signal near the crack tip could be affected by crack closure effect and then the effective stress intensity factor range

would be lower. Clearly, the less robust formulations based on Westergaard' are not affected by this effect because they are less sensitive to local stress state variations.

Table 3. (a) ΔK_I estimated for (a) sample 1 and (b) sample 2.

(a)

	SIF range - ΔK_I [MPa$\sqrt{m}$]				
Analysed sequence	FEM	Stanley-Chan	TSA_ODM_West	TSA_ODM_West+T-stress	TSA_ODM_Will
Sequence 1	40.9	39.0	30.6	23.0	22.8
Sequence 2	42.7	42.0	29.8	17.1	17.0
Sequence 3	45.0	39.0	31.2	20.7	20.3
Sequence 4	46.7	45.0	32.0	23.0	23.0
Sequence 5	51.1	50.0	29.2	19.0	19.1
Sequence 6	66.8	53.0	40.6	37.2	36.9

(b)

	SIF range - ΔK_I [MPa$\sqrt{m}$]				
Analysed sequence	FEM	Stanley-Chan	TSA_ODM_West	TSA_ODM_West+T-stress	TSA_ODM_Will
Sequence 1	21.7	16.9	25.5	16.8	17.0
Sequence 2	22.8	19.2	25.8	11.4	11.5
Sequence 3	26.4	22.2	29.2	12.6	12.6
Sequence 4	28.3	24.0	23.4	14.8	14.9
Sequence 5	35.4	29.9	26.7	18.8	18.9
Sequence 6	39.5	39.0	26.6	22.9	22.3
Sequence 7	42.0	42.4	22.8	19.7	20.6

5.2. Paris'-law like assessment

The results show that the major part of the points lie in the 95% confidence bounds associated with the fitting coefficients of the data series (ΔK_I via FEM vs CGR Optical Microscope).

In particular, the Stanley-Chan' method to evaluate ΔKI combined with the CGR obtained by using the φ_1 and φ_2 inversion points to estimate the crack tips, provides results in good agreement with the reference curve (ΔK_I via FEM vs CGR Optical Microscope).

Over-deterministic method combined with Westergaard' solution provides scattered data that belong to confidence interval just for some points. While more robust Williams solutions data are noisier and sometimes out of the confidence bounds due to a broad underestimation of SIF.

This systematically lower values in SIF values provided by ODMs may be due to the influence of the half cycle in compression where the crack-closure effect could influence negatively the least square fitting. In this way, further work is required to understand better such an influence on ODMs.

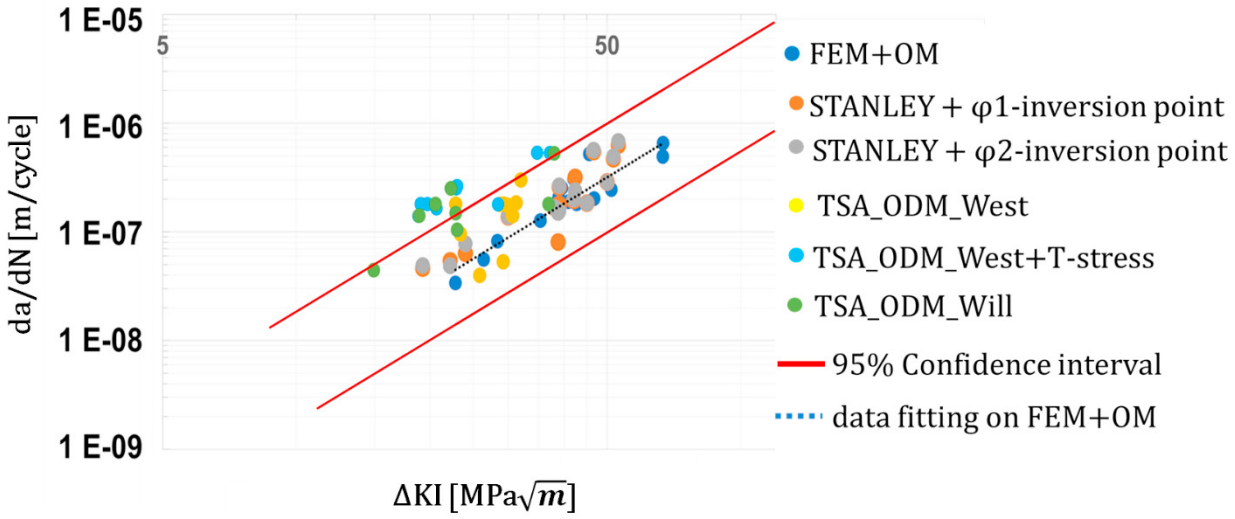

Fig. 9. Paris'-like laws obtained by using TSA-based methods (double logarithmic scale).

6. Conclusions

In this work, two Single Edge Notched Tension samples have been tested under fully reversed load to study fracture mechanics behaviour. The tests were assisted by optical microscope and an infrared camera, observing opposite sides of the sample faces.

The optical microscope allowed the assessment of the crack tip position.

Temperature scanning of samples surfaces allowed the assessment of thermoelastic data (amplitude and phase) and second-harmonic phase data, useful to evaluate both crack tip positions and stress intensity factor ranges.

ΔT_1, φ_1 and φ_2 maps were used to obtain SIF range and CGR in order to determine a Paris'-like law using different methods:

- Based on direct interpolation method to obtain SIF range from ΔT_1 data (Stanley-Chan' method) and CGR considering the φ_1 and φ_2 point inversions of profiles parallel to crack growth direction and related to the opposite dissipative behaviours in the crack region where plastic zone and crack-closure effect coexist.
- Based on application of the over-deterministic system of equations obtained by combining the general expression of the thermoelastic signal and Westergaard' – Williams' solutions, to obtain crack-tips via a trial-and-error procedure and the parameters describing the stress state near the plastic region (ΔK_I, T_s, A_{I3}).

The outcomes of the present work, are:

- ❖ for SENT samples there is a good agreement in detecting crack tip using optical microscope and TSA-based methods;
- ❖ As to ΔK_I, the results showed that Stanley-Chan' method, even though less robust than ODMs, provided ΔK_I values more in agreement with FEM values;
- ❖ ODM seems to systematically underestimate ΔK_I according to these preliminary analyses. This effect could be due to crack closure effect. However, further analyses are required to investigate such a phenomenon.

References

Ancona, F., De Finis, R., Demelio, G.P., Galietti, U., Palumbo, D. 2016. Study of the plastic behavior around the crack tip by means of thermal methods. Procedia Structural Integrity, 2, pp. 2113–212

Ancona, F., Palumbo, D., De Finis, R., Demelio, G.P., Galietti, U. 2016. Automatic procedure for evaluating the Paris Law of martensitic and austenitic stainless steels by means of thermal methods. Engineering Fracture Mechanics, 163, pp. 206–219

ASTM E 647–00. Standard test method for measurement of fatigue crack growth rates; 2004

Diaz, F.A., Patterson, E.A.; Tomlinson, R.A.; Yates, J.R. 2004. Measuring stress intensity factors during fatigue crack growth using thermoelasticity. Fatigue Fract Eng Mater Struct 26(4), 571-583.

Diaz F.A., E.A. Patterson, J.R. Yates. 2005. Differential Thermography Reveals Crack Tip Behaviour ?, in Proceedings 2005 SEM Annual Conference on Experimental Applied Mechanics, Society for Experimental Mechanics, Portland, OR, USA, 6–9 June 2005, pp. 1413–1419.

F.A. Diaz, E.A. Patterson, J.R. Yates. 2013. Application of thermoelastic stress analysis for the experimental evaluation of the effective stress intensity factor. Fracture and Structural Integrity 25, 109-116.

Díaz, F.A., Yates, J.R., Patterson, E.A., 2004a. Some Improvements in the Analysis of Fatigue Cracks Using Thermoelasticity. International Journal of Fatigue 26 (4), 365–76.

Dowling NE, Kampe SL, Milo VK. 2020. Mechanical Behaviour of Materials. 5th Edition, Global edition. Pearson Education Limited 2020 United Kingdom

De Finis, R., Palumbo, D., Ancona, F., Galietti, U. 2017. Fatigue behaviour of stainless steels: A multi-parametric approach. Conference Proceedings of the Society for Experimental Mechanics Series, 9, pp. 1–8

Di Carolo F., R. De Finis, D. Palumbo, U. Galietti, A Thermoelastic Stress Analysis General Model: Study of the influence of Biaxial Residual Stress on Aluminium and Titanium, Metals 9(6) (2019), 671.

Dulieu-Barton, J.M., Worden, J.M. 2003. Genetic identification of crack-tip parameters using thermoelastic isopachics, Meas Sci Technol 14, 176-183.

Gupta, M. , Alderliesten, R.C. , Benedictus, R.2015. A review of T-stress and its effects in fracture mechanics, Eng Fract Mech 134, 218-241.

Lazzarin, P., Berto, F., Zappalorto, M. 2010. Rapid calculations of notch stress intensity factors based on averaged strain energy density from coarse meshes: Theoretical bases and applications. International Journal of Fatigue 32(10), 1559-1567

Lesniak, J.R. and Boyce, B.R.. 1995. Differential Thermography Applied to Structural Integrity Assessment. In SPIE 2473, Thermosense XVII, An International Conference on Thermal Sensing and Imaging Diagnostic Applications, 2473, 2411–73

Meneghetti, G., Lazzarin, P. 2007. Significance of the Elastic Peak Stress Evaluated by FE Analyses at the Point of Singularity of Sharp VNotched Components. Fatigue & Fracture of Engineering Materials & Structures 30 (2), 95–106

Meneghetti, G., Ricotta, M, Pitarresi, G. 2019. Infrared thermography-based evaluation of the elastic-plastic J-integral to correlate fatigue crack growth data of a stainless steel. International Journal of Fatigue 125, 149–160

Palumbo, D., Ancona, F., De Finis, R., Galietti, U. 2015. Experimental Study of the Crack Growth in Stainless Steels Using Thermal Methods.. Procedia Engineering, 109, pp. 338–345G.

Patterson ,E.A. 2007. The Potential for Quantifying Residual Stress Using Thermoelastic Stress Analysis, in Proceedings of the SEM Annual Conference and Exposition on Experimental and Applied Mechanics 2007, Springfield, MA; USA, 3–6 June 2007; pp. 664–669.

Paul S.K., Tarafder,S 2012. Cyclic plastic deformation response at fatigue crack tips. International Journal of Pressure Vessels and Piping xxx, 1e10.

Pitarresi, M. Ricotta, G. Meneghetti, Investigation of the crack tip stress field in a stainless steel SENT specimen by means of thermoelastic stress analysis. Procedia Struct Integr 18 (2019) 330-346.

Stanley, P. 1997 Applications and potential of thermoelastic stress analysis, J Mater Process Tech 64, 359-370.

Tomlinson, R.A., Nurse, A.D. , Patterson, E.A. 1997. On determining stress intensity factors for mixed mode cracks from thermoelastic data, Fatigue Fract Engng Mater Struct 20(2), 217-226.

Tomlinson, R.A., Olden, E.J. 1999. Thermoelasticity for the analysis of crack tip stress fields – review, Strain 35 (1999), 49-55.

Tomlinson, R.A., Patterson, E.A. 2011. Examination of Crack Tip Plasticity Using Thermoelastic Stress analysis, Thermomechanics and Infra-Red Imaging, in: Proceedings of the Society for Experimental Mechanics Series 2011, Volume 7, Springer, New York, NY.

Vasco-Olmo, J.M. , James, M.N. , Christoper, C.J. , Patterson, E.A. .2016. Assessment of crack tip plastic zone size and shape and its influence on crack tip shielding, Fatigue Fract Eng Mater Struct 39, 969-981.

William Thomson, M.A.1878. On the thermoelastic, thermomagnetic, and pyroelectric properties of matter, The London, Edinburgh, and Dublin Philosophical Magazine and Journal of Science 1878, 5(28), Series 5.

Yates, J.R., Zanganeh, M. 2010.Quantifying crack tip displacement fields with DIC, Eng Fract Mech 77(11), 2063-2076.